Letter

Principal deuterium Hugoniot via quantum Monte Carlo and Δ-learning

Giacomo Tenti [1,*] Kousuke Nakano [2,†] Andrea Tirelli,[1] Sandro Sorella,[1] and Michele Casula [3,‡]

[1]*International School for Advanced Studies (SISSA), Via Bonomea 265, 34136 Trieste, Italy*
[2]*Center for Basic Research on Materials, National Institute for Materials Science (NIMS), Tsukuba, Ibaraki 305-0047, Japan*
[3]*Institut de Minéralogie, de Physique des Matériaux et de Cosmochimie (IMPMC), Sorbonne Université, CNRS UMR 7590,
MNHN, 4 Place Jussieu, 75252 Paris, France*

We present a study of the principal deuterium Hugoniot for pressures up to 150 GPa, using machine learning potentials (MLPs) trained with quantum Monte Carlo (QMC) energies, forces, and pressures. In particular, we adopted a recently proposed workflow based on the combination of Gaussian kernel regression and Δ-learning. By fully taking advantage of this method, we explicitly considered finite-temperature electrons in the dynamics, whose effects are highly relevant for temperatures above 10 kK. The Hugoniot curve obtained by our MLPs shows a good agreement with the most recent experiments, particularly in the region below 60 GPa. At larger pressures, our Hugoniot curve is slightly more compressible than the one yielded by experiments, whose uncertainties generally increase, however, with pressure. Our work demonstrates that QMC can be successfully combined with Δ-learning to deploy reliable MLPs for complex extended systems across different thermodynamic conditions, by keeping the QMC precision at the computational cost of a mean-field calculation.

DOI: 10.1103/PhysRevB.110.L041107

Introduction. The study of hydrogen under extreme conditions has been a very active topic in condensed matter physics. Hydrogen is the most abundant element in the universe and the accurate knowledge of its phase diagram at pressures of the order of hundreds of GPa is extremely important for a variety of applications, such as modeling the interior of stars and giant gas planets [1–3], the inertial-confinement fusion [4], and the high-T_c hydrogen-based superconductors [5,6]. Nevertheless, several properties of this system are still highly debated, even at the qualitative level [7–10].

One of the main reasons that hamper our full understanding of high-pressure hydrogen is the difficulty of reproducing extreme pressures in a laboratory. Typical shock-wave experiments [11] make use of accelerated flyer plates to compress a material sample in a very short time, thus allowing the study of specimens at high temperatures and pressures. In particular, the set of possible end states that the system can reach from some given initial conditions, also named the principal Hugoniot, must satisfy a set of equations, known as the Rankine-Hugoniot (RH) relations [12], linking the thermodynamic properties of the final shocked state with those of the starting one. During the years, the principal deuterium Hugoniot has been measured for a wide range of pressures and with a great degree of accuracy [13–20], particularly in the lower pressure ($\lesssim 60$ GPa) region, where the relative error on the density is as small as 2% in recent experiments.

In this context, numerical approaches, in particular *ab initio* molecular dynamics (AIMD) simulations, are extremely valuable, since they are not constrained by any

experimental setup and can thus give further insight into this part of the phase diagram [21]. The Hugoniot region is particularly important because of the availability of experimental data that can be used to benchmark different theoretical methods. Among them, density functional theory (DFT) has been extensively applied to compute the Hugoniot curve [22–28]. In this framework, the approximations behind the particular exchange-correlation functional often produce discrepancies across existing DFT schemes, whose accuracy varies according to the thermodynamic conditions. Quantum Monte Carlo (QMC) simulations, which depend on more controllable approximations, have also been performed [29,30]. Although in principle more accurate and systematically improvable, these calculations have a much larger computational cost than DFT, and they are thus limited in system size and simulation length. Moreover, previous QMC calculations [29] seem to give results for the principal Hugoniot in disagreement with the most recent experimental data, with the possible origin of this discrepancy being recently debated [31]. However, the most recent QMC results [30] are closer to the experimental curve, particularly at low compression.

To overcome the large computational cost of *ab initio* simulations, machine learning techniques, aimed at constructing accurate potential energy surfaces, have become increasingly popular. Within this approach, one uses a dataset of configurations, i.e., the training set, to build a machine learning potential (MLP) that is able to reproduce energies and forces calculated with the given target method [32]. Unlike DFT MLPs, the QMC ones are relatively less common, given the larger computational cost and the consequent difficulty of generating extended datasets, usually necessary to construct accurate MLPs.

In this work, we have built an accurate MLP using QMC energies, forces, and pressures in the region of the

_____

*Contact author: gtenti@sissa.it
†Contact author: kousuke_1123@icloud.com
‡Contact author: michele.casula@upmc.fr

deuterium Hugoniot, using the so-called Δ-learning approach. The Hugoniot curve computed by our QMC-MLP shows an excellent agreement with the most recent experiments at low density, while presenting a slightly larger compressibility for temperatures above 10 kK, where the experimental points are also affected by larger error bars.

Computational details. In order to build an MLP with QMC references, we employed a combination of Gaussian kernel regression (GKR), smooth overlap of atomic positions (SOAP) descriptors [33], and Δ-learning. The same approach has been recently proposed in Ref. [34], where it was applied to the study of high-pressure hydrogen in similar thermodynamic conditions. Following the Δ-learning approach, an MLP is trained on the difference between the target method and a usually much cheaper baseline potential. Here, we trained several MLPs, using variational Monte Carlo (VMC) and lattice regularized diffusion Monte Carlo (LRDMC) [35,36] datapoints as targets, and two different DFT baselines, with the Perdew-Zunger local density approximation (PZ-LDA) [37] and the Perdew-Burke-Ernzerhof (PBE) [38] functionals.

To determine the principal Hugoniot, we made use of the RH jump equation:

$$H(\rho, T) = e(\rho, T) - e_0 + \frac{1}{2}(\rho^{-1} - \rho_0^{-1})[p(\rho, T) + p_0] = 0, \tag{1}$$

where ρ, T, $e(\rho, T)$, $p(\rho, T)$, and ρ_0, T_0, e_0, p_0 are the density, temperature, energy per particle, and pressure of the final and initial states, respectively. In particular, we ran a first set of NVT simulations for a system of $N = 128$ atoms at several temperatures in the [4 kK : 8 kK] range, and Wigner-Seitz radii between 1.80 Bohr and 2.24 Bohr, corresponding to the range where the zero of $H(\rho, T)$ was expected. These simulations were performed considering classical nuclei and ground-state electrons, as quantum corrections and thermal effects have been shown to be negligible for these temperatures [30]. At each step, the energy, forces, and pressure were calculated using the QUANTUM ESPRESSO package in its GPU accelerated version [39–41] with the chosen functional (PBE in most cases), and then corrected with our MLP trained on the difference between QMC and DFT data. The resulting dynamics has the same efficiency as a standard DFT AIMD simulation, which is roughly 100 times faster than the original QMC one. For the DFT simulations, we considered a 60 Ry plane-wave cutoff with a projector augmented wave (PAW) pseudopotential [42] and a $4 \times 4 \times 4$ Monkhorst-Pack k-point grid, while for the dynamics we used a time step of 0.25 fs and a Langevin thermostat [43,44] with damping $\gamma = 0.13\,\text{fs}^{-1}$. For each temperature, the Hugoniot (ρ^*, p^*) coordinates are determined by fitting the Hugoniot function $H(\rho, T)$ and the pressure $p(\rho, T)$ with a spline function, and by numerically finding ρ^* and the corresponding p^*.

The QMC calculations were performed using the TURBORVB package [45,46]. When generating our QMC-MLP model, we took particular care to the training set construction, based on energies, forces, and pressures all computed at the QMC (VMC or LRDMC) level. In general, QMC forces and pressure are not guaranteed to be consistent with the relative potential energy surface, due to the practical difficulty of optimizing all the parameters within a given ansatz

for the VMC wave function (WF). This is often called self-consistency error [47–49]. Even if ML frameworks generally satisfy the consistency property by construction, the presence of biased forces and pressure in the training can spoil the accuracy of the model and produce, in principle, unintended results. Therefore, to avoid these issues, we mitigated the self-consistency error by directly optimizing not only the Jastrow factor but also the determinantal part of the VMC WF. The details of our QMC simulations are reported in the Supplemental Material (SM) [50].

Within our approach, we can fully take advantage of the Δ-learning method by estimating the effect of thermalized electrons in our calculations. To do so, we ran simulations at temperatures $T = 10$ kK, 15 kK, 20 kK, and 35 kK considering the effect of finite T in the underlying PBE energies and forces. In this way, we can include the effects of thermally excited electrons in our MLP without changing it, at least at the DFT level of theory. Here, the effect of the explicit dependence of the DFT functional on T was not considered, since it has been shown to be negligible for hydrogen systems and the temperature range analyzed here [28,51,52]. We remark that this approach is also applicable when a DFT-MLP is used as a baseline in place of an *ab initio* calculation, where finite temperature effects can be estimated from the DFT density of states [53].

Results and discussion. Figure 1(a) shows our results together with several experimental values for pressures below 150 GPa [16,19,20]. We also report the principal Hugoniot obtained by directly using the PBE baseline and the coupled electron ion Monte Carlo (CEIMC) results of Ref. [30] for comparison. For temperatures larger than $T = 10$ kK the results refer to the MDs obtained using finite temperature DFT as a baseline. Both the VMC and LRDMC models give a very similar Hugoniot line, well reproducing the experimental points in the low density—low pressure region. With respect to the most accurate data of Ref. [19], our estimate of the relative density ρ/ρ_0 at the compressibility peak is ∼3–4% larger, still within the error bars. For larger pressures, we predict a Hugoniot mostly compatible within the experiments but systematically more compressible. However, in this regime the correspondingly larger uncertainties in the measures prevent a clear-cut assessment of our outcome. Our results also agree with the most recent low-temperature CEIMC ones reported in Ref. [30] within the statistical accuracy.

Figure 1(b) displays the same points in the $u_p - U_s$ space, where u_p is the particle velocity and U_s is the shock velocity, the two being calculated using the following RH relations:

$$u_p = \sqrt{(p + p_0)(\rho_0^{-1} - \rho^{-1})},$$

$$U_s = \rho_0^{-1}\sqrt{\frac{p + p_0}{\rho_0^{-1} - \rho^{-1}}}.$$

The difference ΔU_s between these points and the linear fit on the gas-gun data reanalyzed in Ref. [19] is also shown (bottom panel of Fig. 1(b)). The drop in the slope of U_s relative to u_p coincides with the onset of the molecular-atomic (MA) transition, while the magnitude of the ΔU_s minimum relates to the position of the relative compression peak. In particular, the PBE Hugoniot curve manifests a premature start of the
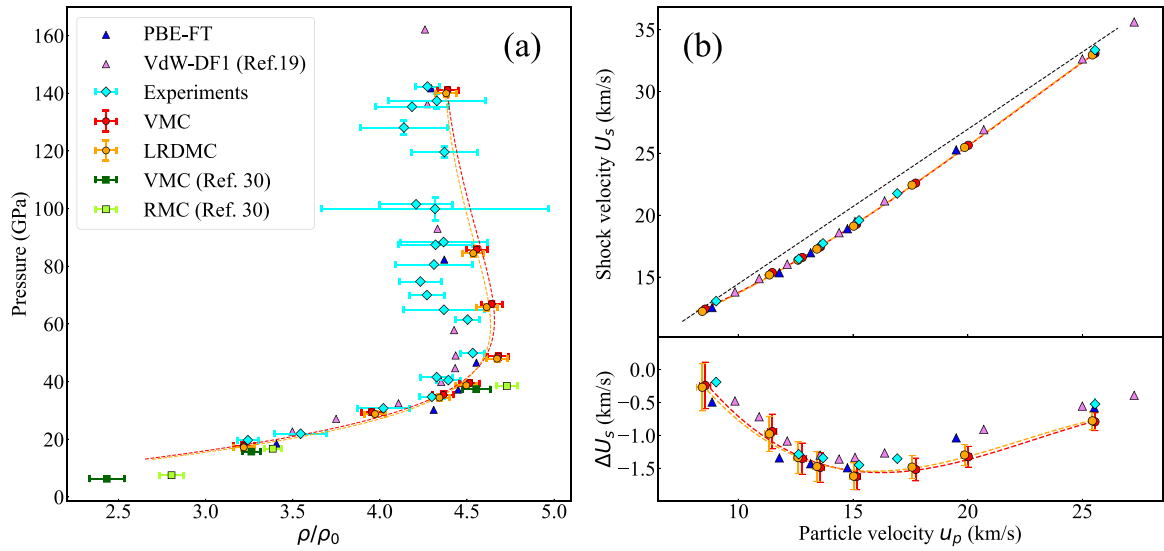
FIG. 1. (a) Principal Hugoniot in the density-pressure space. Red and yellow circles are the results obtained with our MLPs trained on VMC and LRDMC datapoints, respectively, and a PBE baseline. Blue and pink triangles are the PBE result calculated in this work and the VdW-DF1 result of Ref. [19], respectively. CEIMC results of Ref. [30] based on variational Monte Carlo (VMC) and reptation Monte Carlo (RMC) are reported in green squares. Cyan diamonds are the experimental results of Refs. [16,19,20]. Dashed lines are guides for the eye. (b) [top panel] Hugoniot in the u_p–U_s space. The black dashed line is the reanalyzed gas-gun fit reported in Ref. [19], i.e., the shock velocity extrapolated from measures of molecular deuterium at low pressure [13]. (b) [Bottom panel] Relative shock velocity with respect to the gas-gun fit. Only the experimental points of Ref. [19] are reported.

dissociation, while it predicts correctly the magnitude of the compressibility maximum. Our QMC results correctly predict the position of the peak and starting slope, while showing some discrepancies for $u_p \gtrsim 15$ km/s with respect to the data of Ref. [19]. In this regime, DFT, and in particular the result obtained with the VdW-DF1 functional [54,55], seems to be in better agreement with experiments, thanks to a favorable error cancellation in the Hugoniot [31]. We noticed how, in this study, the discrepancy with the experiments is much milder than the value reported by previous QMC calculations at densities and pressures close to the compressibility peak [29]. This can be due to the explicit optimization of the WF nodal surface provided by our WF ansatz, which reduces the fixed node error mentioned in Ref. [31], the only approximation left in any projective Monte Carlo calculation, such as LRDMC and RMC. The difference between the various methods is also apparent in their equations of state, reported in the SM [50].

The presence of an MA transition is investigated in Fig. 2, where we report the radial distribution function, $g(r)$, calculated on trajectories obtained with the LRDMC model for several temperatures at densities close to the Hugoniot curve. The inset of Fig. 2 displays the value of the molecular fraction m, defined as the percentage of atoms that stay within a distance of 2 Bohr [roughly corresponding to the first $g(r)$ minimum after the molecular peak] from another particle for longer than a characteristic time, here set to 6 fs. The results indicate a distinct atomic character for $T \geqslant 10$ kK and a clear molecular peak at lower temperatures. The LRDMC model shows a larger molecular fraction than the PBE and VdW-DF1 ones, being compatible with the latter for temperatures above 10 kK.
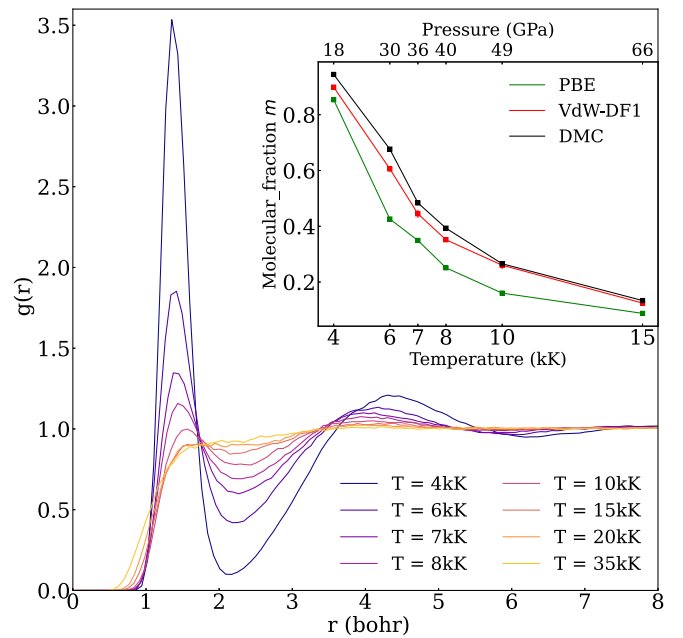

FIG. 2. $g(r)$ for several temperatures and densities close to the principal Hugoniot, obtained using the LRDMC model. The molecular fraction value, m, is reported in the inset for each value of temperature up to 15 kK. On the top axis the corresponding pressure at the Hugoniot is also shown. The values obtained with an *ab initio* DFT dynamics using the PBE and VdW-DF1 functionals are reported for comparison at the same temperatures (notice that a pressure and density mismatch between methods can be present in this case due to different equations of state).

Error analysis. To assess the quality of our principal Hugoniot determination, we analyzed the possible sources of errors in relation to our machine learning scheme. There are three main sources of errors: the uncertainties in the fit of $H(\rho, T)$, the prediction error of the MLP, and the uncertainties in the reference state energy estimate, i.e., e_0 in Eq. (1). We verified that, in our case, the error produced by the fit is negligible compared to the other two sources, which we will discuss next.

As mentioned before, we followed Ref. [34] to construct our MLPs and used a GKR model based on a modified version of the SOAP kernel [33]. Our final dataset, including both training and test sets, comprises 561 configurations selected through an iterative procedure with 128 hydrogen atoms each, where we calculated energies, pressures, and forces at the VMC and LRDMC levels. These configurations correspond to temperatures from 4 kK up to 20 kK and Wigner-Seitz radii from 1.80 Bohr to 2.12 Bohr. Finite size corrections (FSC) have also been estimated using the KZK functional [56]. Details on the training set construction and the QMC calculations, together with the performances of all MLP models can be found in the SM [50]. In particular we found a final root mean square error (RMSE), calculated on the test set, of the order of 7 meV/atom for the energy, 250 meV/Å for the forces, and 0.75 GPa for the pressures.

At this point, it is worth to highlight some favorable features of our machine learning approach, especially in applications where it is coupled with computationally expensive methods such as QMC. They can be itemized as follows:

(i) *Transferability*: the total energy of the system is expressed as a sum of local terms [32], therefore our models are capable of making accurate predictions on configurations whose size has never been encountered in the training set. In particular, our MLPs find their applicability to systems with an arbitrary number of atoms N.

(ii) *Efficiency and accuracy*: within the Δ-learning framework, the machine learning task becomes easier. Indeed, we obtained very accurate QMC potentials, by training models on small datasets and, thus, by reducing the amount of calculations needed. Moreover, since the computational cost of the ML inference is negligible compared to the baseline DFT calculation, we were able to perform QMC-driven MD simulations at the cost of a DFT dynamics.

(iii) *Overfitting prevention*: using a local sparsification technique based on the farthest point sampling (see the SM of Ref. [34]), we discarded from each configuration a possibly large fraction of the corresponding N local environments, preventing overfitting and allowing for an increased predictive power of the model on unseen data. Since the computational cost of the predictions scales with the size of the training set, this procedure drastically improves the efficiency of the final model.

We further validated the accuracy of our MLPs by comparing the Hugoniot curve obtained using two potentials, independently trained with the same target, e.g., VMC, but with two different baselines. Taking into account these results and the RMSE of the models, we can estimate an uncertainty on the prediction of 0.06 on the relative density ρ/ρ_0 and 1 GPa on pressure.

TABLE I. Estimated potential (e_{pot}) and total (e_0) energies per atom of the reference state at $\rho_0 = 0.167$ g/cm^3 and $T = 22$ K for different methods, with and without finite size corrections (FSC).

	e_{pot} (Ha/atom)	e_0 (Ha/atom)
PBE	−0.582 17(2)	−0.580 55(2)
VMC	−0.586 22(2)	−0.584 60(2)
LRDMC	−0.586 60(2)	−0.584 98(2)
VMC + FSC	−0.585 03(2)	−0.583 42(2)
LRDMC + FSC	−0.585 42(2)	−0.583 80(2)

We now turn to the last source of error we identified, i.e., the one related to the calculation of e_0 and p_0. To estimate the reference state energy and pressure, we followed a procedure similar to Ref. [30]. We performed a path integral molecular dynamics (PIMD) simulation [57] on a system of $N = 64$ deuterium atoms at a temperature $T = 22$ K and density $\rho_0 = 0.167$ g/cm^3 (corresponding to the initial conditions reported in Ref. [19]), using DFT-PBE energy and forces. Details of this simulation are reported in the SM [50]. From the PIMD trajectory, we extracted 170 configurations and we calculated energies and pressures with both DFT-PBE and QMC at VMC and LRDMC levels, adding the necessary finite size corrections. The reference sample was generated by extracting atomic positions from one of the 128 beads taken at random, belonging to decorrelated snapshots of the trajectory. Results for e_0 for the various methods are reported in Table I. The reference state pressure p_0 is not reported, since it is two orders of magnitude smaller than the shocked pressure, and thus irrelevant for the Hugoniot determination. Also in this case, we studied the effect of varying e_0 within its confidence interval on the Hugoniot density and pressure. In doing so, we also took into account the possible uncertainty on the energy difference $e(\rho, T) - e_0$ originating by the finite batch size we used for estimating energy gradients in the WF optimization. We estimated this uncertainty by running optimizations of increasing batch size on three different 128-atom configurations. The results indicate an error $\lesssim 0.5$ mHa/atom on $e(\rho, T) - e_0$. Taking everything into account, varying the energy within standard deviation leads to shifts in the final principal Hugoniot which still fall in the error bars of our predictions estimated previously.

To summarize, we estimated the MLP prediction error to be the most relevant source of uncertainty for the Hugoniot, yielding, as discussed before, an absolute error of 0.06 and 1 GPa on the relative density and pressure, respectively, reflected on the error bars reported in Fig. 1.

Conclusions. In conclusion, using our recently proposed workflow for the construction of MLPs, we have been able to run reliable VMC- and LRDMC-based MD simulations and study the principal deuterium Hugoniot, in a pressure range relevant for experiments. The accuracy of the MLPs employed here has been extensively tested, supporting the validity of our calculations and estimating their uncertainty. The resulting Hugoniot curve shows generally good agreement with the most recent experimental measures, especially in the low temperature molecular regime. Exploiting the Δ-learning

framework, we have also been able to treat FT electrons effects in a QMC-MLP, and we have thus managed to perform accurate simulations at higher temperatures. For these temperatures, the results systematically show a more compressible Hugoniot curve than experiments, although the experimental error bars are large in this regime. The aforementioned discrepancy is milder than previously reported QMC calculations [29], and falls within the measures uncertainty. In particular, this suggests that the use of optimized and more refined WFs has a key role for obtaining good results in high-pressure hydrogen. We thus believe that our results will be useful for both future experimental research and numerical investigations of the Hugoniot. The efficiency of our computational approach could be further improved, e.g., by using cheaper baseline potentials than DFT. Longer simulations and larger systems will then be at reach. Other many-body methods, even more expensive than QMC, can also be used as targets for this type of MLPs, since the required size of the dataset is at least one order of magnitude smaller compared to other ML approaches. Finally, our MLPs, and in particular those trained on LRDMC data points, are promising for exploring the hydrogen phase diagram by keeping a high level of accuracy across a wide range of thermodynamic conditions.

The machine learning code used in this work is available upon request. Additional information, such as datasets, models, and detailed results of the simulations are available at [70].

---

[1] D. Saumon, G. Chabrier, and H. M. van Horn, An equation of state for low-mass stars and giant planets, Astrophys. J. Suppl. Ser. **99**, 713 (1995).

[2] J. J. Fortney and N. Nettelmann, The interior structure, composition, and evolution of giant planets, Space Sci. Rev. **152**, 423 (2010).

[3] Y. Miguel, T. Guillot, and L. Fayon, Jupiter internal structure: The effect of different equations of state, Astron. Astrophys. **596**, A114 (2016).

[4] S. X. Hu, V. N. Goncharov, T. R. Boehly, R. L. McCrory, S. Skupsky, L. A. Collins, J. D. Kress, and B. Militzer, Impact of first-principles properties of deuteriumtritium on inertial confinement fusion target designs, Phys. Plasmas **22**, 056304 (2015).

[5] A. P. Drozdov, M. I. Eremets, I. A. Troyan, V. Ksenofontov, and S. I. Shylin, Conventional superconductivity at 203 kelvin at high pressures in the sulfur hydride system, Nature (London) **525**, 73 (2015).

[6] M. Somayazulu, M. Ahart, A. K. Mishra, Z. M. Geballe, M. Baldini, Y. Meng, V. V. Struzhkin, and R. J. Hemley, Evidence for superconductivity above 260 K in lanthanum superhydride at megabar pressures, Phys. Rev. Lett. **122**, 027001 (2019).

[7] J. M. McMahon, M. A. Morales, C. Pierleoni, and D. M. Ceperley, The properties of hydrogen and helium under extreme conditions, Rev. Mod. Phys. **84**, 1607 (2012).

[8] B. Cheng, G. Mazzola, C. J. Pickard, and M. Ceriotti, Evidence for supercritical behaviour of high-pressure liquid hydrogen, Nature (London) **585**, 217 (2020).

[9] V. V. Karasiev, J. Hinz, S. X. Hu, and S. B. Trickey, On the liquid-liquid phase transition of dense hydrogen, Nature (London) **600**, E12 (2021).

[10] B. Cheng, G. Mazzola, C. J. Pickard, and M. Ceriotti, Reply to: On the liquid-liquid phase transition of dense hydrogen, Nature (London) **600**, E15 (2021).

[11] W. J. Nellis, Dynamic compression of materials: Metallization of fluid hydrogen at high pressures, Rep. Prog. Phys. **69**, 1479 (2006).

[12] G. E. Duvall and R. A. Graham, Phase transitions under shockwave loading, Rev. Mod. Phys. **49**, 523 (1977).

[13] W. J. Nellis, A. C. Mitchell, M. van Thiel, G. J. Devine, R. J. Trainor, and N. Brown, Equation of state data for molecular hydrogen and deuterium at shock pressures in the range 2–76 GPa (20–760 kbar), J. Chem. Phys. **79**, 1480 (1983).

[14] M. D. Knudson, D. L. Hanson, J. E. Bailey, C. A. Hall, J. R. Asay, and W. W. Anderson, Equation of state measurements in liquid deuterium to 70 GPa, Phys. Rev. Lett. **87**, 225501 (2001).

[15] G. V. Boriskov, A. I. Bykov, R. I. Il'kaev, V. D. Selemir, G. V. Simakov, R. F. Trunin, V. D. Urlin, A. N. Shuikin, and W. J. Nellis, Shock compression of liquid deuterium up to 109 GPa, Phys. Rev. B **71**, 092104 (2005).

[16] M. D. Knudson, D. L. Hanson, J. E. Bailey, C. A. Hall, J. R. Asay, and C. Deeney, Principal Hugoniot, reverberating wave, and mechanical reshock measurements of liquid deuterium to 400 GPa using plate impact techniques, Phys. Rev. B **69**, 144209 (2004).

[17] D. G. Hicks, T. R. Boehly, P. M. Celliers, J. H. Eggert, S. J. Moon, D. D. Meyerhofer, and G. W. Collins, Laser-driven

single shock compression of fluid deuterium from 45 to 220 GPa, Phys. Rev. B **79**, 014112 (2009).

[18] P. Loubeyre, S. Brygoo, J. Eggert, P. M. Celliers, D. K. Spaulding, J. R. Rygg, T. R. Boehly, G. W. Collins, and R. Jeanloz, Extended data set for the equation of state of warm dense hydrogen isotopes, Phys. Rev. B **86**, 144115 (2012).

[19] M. D. Knudson and M. P. Desjarlais, High-precision shock wave measurements of deuterium: Evaluation of exchange-correlation functionals at the molecular-to-atomic transition, Phys. Rev. Lett. **118**, 035501 (2017).

[20] A. Fernandez-Pañella, M. Millot, D. E. Fratanduono, M. P. Desjarlais, S. Hamel, M. C. Marshall, D. J. Erskine, P. A. Sterne, S. Haan, T. R. Boehly, G. W. Collins, J. H. Eggert, and P. M. Celliers, Shock compression of liquid deuterium up to 1 TPa, Phys. Rev. Lett. **122**, 255702 (2019).

[21] M. D. Knudson and M. P. Desjarlais, Interplay of high-precision shock wave experiments with first-principles theory to explore molecular systems at extreme conditions: A perspective, J. Appl. Phys. **129**, 210904 (2021).

[22] T. J. Lenosky, S. R. Bickham, J. D. Kress, and L. A. Collins, Density-functional calculation of the Hugoniot of shocked liquid deuterium, Phys. Rev. B **61**, 1 (2000).

[23] G. Galli, R. Q. Hood, A. U. Hazi, and F. Gygi, *Ab initio* simulations of compressed liquid deuterium, Phys. Rev. B **61**, 909 (2000).

[24] S. Bagnier, P. Blottiau, and J. Clérouin, Local-spin-density-approximation molecular-dynamics simulations of dense deuterium, Phys. Rev. E **63**, 015301(R) (2000).

[25] S. A. Bonev, B. Militzer, and G. Galli, *Ab initio* simulations of dense liquid deuterium: Comparison with gas-gun shock-wave experiments, Phys. Rev. B **69**, 014101 (2004).

[26] B. Holst, R. Redmer, and M. P. Desjarlais, Thermophysical properties of warm dense hydrogen using quantum molecular dynamics simulations, Phys. Rev. B **77**, 184201 (2008).

[27] L. Caillabet, S. Mazevet, and P. Loubeyre, Multiphase equation of state of hydrogen from *ab initio* calculations in the range 0.2 to 5 g/cc up to 10 eV, Phys. Rev. B **83**, 094101 (2011).

[28] V. V. Karasiev, S. X. Hu, M. Zaghoo, and T. R. Boehly, Exchange-correlation thermal effects in shocked deuterium: Softening the principal Hugoniot and thermophysical properties, Phys. Rev. B **99**, 214110 (2019).

[29] N. M. Tubman, E. Liberatore, C. Pierleoni, M. Holzmann, and D. M. Ceperley, Molecular-atomic transition along the deuterium Hugoniot curve with coupled electron-ion Monte Carlo simulations, Phys. Rev. Lett. **115**, 045301 (2015).

[30] M. Ruggeri, M. Holzmann, D. M. Ceperley, and C. Pierleoni, Quantum Monte Carlo determination of the principal Hugoniot of deuterium, Phys. Rev. B **102**, 144108 (2020).

[31] R. C. Clay III, M. P. Desjarlais, and L. Shulenburger, Deuterium Hugoniot: Pitfalls of thermodynamic sampling beyond density functional theory, Phys. Rev. B **100**, 075103 (2019).

[32] J. Behler and M. Parrinello, Generalized neural-network representation of high-dimensional potential-energy surfaces, Phys. Rev. Lett. **98**, 146401 (2007).

[33] S. De, A. P. Bartók, G. Csányi, and M. Ceriotti, Comparing molecules and solids across structural and alchemical space, Phys. Chem. Chem. Phys. **18**, 13754 (2016).

[34] A. Tirelli, G. Tenti, K. Nakano, and S. Sorella, High-pressure hydrogen by machine learning and quantum Monte Carlo, Phys. Rev. B **106**, L041105 (2022).

[35] M. Casula, C. Filippi, and S. Sorella, Diffusion Monte Carlo method with lattice regularization, Phys. Rev. Lett. **95**, 100201 (2005).

[36] K. Nakano, R. Maezono, and S. Sorella, Speeding up *ab initio* diffusion Monte Carlo simulations by a smart lattice regularization, Phys. Rev. B **101**, 155106 (2020).

[37] J. P. Perdew and A. Zunger, Self-interaction correction to density-functional approximations for many-electron systems, Phys. Rev. B **23**, 5048 (1981).

[38] J. P. Perdew, K. Burke, and M. Ernzerhof, Generalized gradient approximation made simple, Phys. Rev. Lett. **77**, 3865 (1996).

[39] P. Giannozzi, S. Baroni, N. Bonini, M. Calandra, R. Car, C. Cavazzoni, D. Ceresoli, G. L. Chiarotti, M. Cococcioni, I. Dabo, A. D. Corso, S. de Gironcoli, S. Fabris, G. Fratesi, R. Gebauer, U. Gerstmann, C. Gougoussis, A. Kokalj, M. Lazzeri, L. Martin-Samos *et al.*, QUANTUM ESPRESSO: A modular and open-source software project for quantum simulations of materials, J. Phys.: Condens. Matter **21**, 395502 (2009).

[40] P. Giannozzi, O. Andreussi, T. Brumme, O. Bunau, M. B. Nardelli, M. Calandra, R. Car, C. Cavazzoni, D. Ceresoli, M. Cococcioni, N. Colonna, I. Carnimeo, A. D. Corso, S. de Gironcoli, P. Delugas, R. A. DiStasio, A. Ferretti, A. Floris, G. Fratesi, G. Fugallo, et al., Advanced capabilities for materials modelling with quantum ESPRESSO, J. Phys.: Condens. Matter **29**, 465901 (2017).

[41] P. Giannozzi, O. Baseggio, P. Bonfà, D. Brunato, R. Car, I. Carnimeo, C. Cavazzoni, S. de Gironcoli, P. Delugas, F. Ferrari Ruffino, A. Ferretti, N. Marzari, I. Timrov, A. Urru, and S. Baroni, Quantum espresso toward the exascale, J. Chem. Phys. **152**, 154105 (2020).

[42] H.pbe-kjpaw_psl.1.0.0.UPF pseudopotential available at http://pseudopotentials.quantum-espresso.org/legacy_tables/ ps-library/h.

[43] A. Ricci and G. Ciccotti, Algorithms for brownian dynamics, Mol. Phys. **101**, 1927 (2003).

[44] C. Attaccalite and S. Sorella, Stable liquid hydrogen at high pressure by a novel *ab initio* molecular-dynamics calculation, Phys. Rev. Lett. **100**, 114501 (2008).

[45] K. Nakano, C. Attaccalite, M. Barborini, L. Capriotti, M. Casula, E. Coccia, M. Dagrada, C. Genovese, Y. Luo, G. Mazzola, A. Zen, and S. Sorella, TurboRVB: A many-body toolkit for *ab initio* electronic simulations by quantum Monte Carlo, J. Chem. Phys. **152**, 204121 (2020).

[46] K. Nakano, O. Kohulák, A. Raghav, M. Casula, and S. Sorella, TurboGenius: Python suite for high-throughput calculations of *ab initio* quantum Monte Carlo methods, J. Chem. Phys. **159**, 224801 (2023).

[47] J. Tiihonen, R. C. Clay III, and J. T. Krogel, Toward quantum Monte Carlo forces on heavier ions: Scaling properties, J. Chem. Phys. **154**, 204111 (2021).

[48] K. Nakano, A. Raghav, and S. Sorella, Space-warp coordinate transformation for efficient ionic force calculations in quantum Monte Carlo, J. Chem. Phys. **156**, 034101 (2022).

[49] K. Nakano, M. Casula, and G. Tenti, Efficient calculation of unbiased atomic forces in *ab initio* variational Monte Carlo, Phys. Rev. B **109**, 205151 (2024).

[50] See Supplemental Material at http://link.aps.org/supplemental/ 10.1103/PhysRevB.110.L041107 for additional information

about the computational details of QMC calculations, MLP training and validation, reference state calculations, finite-size corrections, finite temperature DFT simulations, and comparison with previous results, which includes Refs. [28,30,31,34,35,37,39–41,44,45,47–49,56–69].

[51] V. V. Karasiev, T. Sjostrom, J. Dufty, and S. B. Trickey, Accurate homogeneous electron gas exchange-correlation free energy for local spin-density calculations, Phys. Rev. Lett. **112**, 076403 (2014).

[52] V. V. Karasiev, J. W. Dufty, and S. B. Trickey, Nonempirical semilocal free-energy density functional for matter under extreme conditions, Phys. Rev. Lett. **120**, 076401 (2018).

[53] C. Ben Mahmoud, F. Grasselli, and M. Ceriotti, Predicting hot-electron free energies from ground-state data, Phys. Rev. B **106**, L121116 (2022).

[54] M. Dion, H. Rydberg, E. Schröder, D. C. Langreth, and B. I. Lundqvist, Van der waals density functional for general geometries, Phys. Rev. Lett. **92**, 246401 (2004).

[55] K. Berland, V. R. Cooper, K. Lee, E. Schröder, T. Thonhauser, P. Hyldgaard, and B. I. Lundqvist, Van der waals forces in density functional theory: A review of the vdW-DF method, Rep. Prog. Phys. **78**, 066501 (2015).

[56] H. Kwee, S. Zhang, and H. Krakauer, Finite-size correction in many-body electronic structure calculations, Phys. Rev. Lett. **100**, 126404 (2008).

[57] F. Mouhat, S. Sorella, R. Vuilleumier, A. M. Saitta, and M. Casula, Fully quantum description of the zundel ion: Combining variational quantum Monte Carlo with path integral langevin dynamics, J. Chem. Theory Comput. **13**, 2400 (2017).

[58] M. Casula and S. Sorella, Geminal wave functions with jastrow correlation: A first application to atoms, J. Chem. Phys. **119**, 6500 (2003).

[59] S. Sorella, N. Devaux, M. Dagrada, G. Mazzola, and M. Casula, Geminal embedding scheme for optimal atomic basis set construction in correlated calculations, J. Chem. Phys. **143**, 244112 (2015).

[60] F. Becca and S. Sorella, *Quantum Monte Carlo approaches for correlated systems* (Cambridge University Press, Cambridge, 2017).

[61] K. Nakano, T. Morresi, M. Casula, R. Maezono, and S. Sorella, Atomic forces by quantum Monte Carlo: Application to phonon dispersion calculations, Phys. Rev. B **103**, L121110 (2021).

[62] C. J. Umrigar, Two aspects of quantum Monte Carlo: Determination of accurate wavefunctions and determination of potential energy surfaces of molecules, Int. J. Quantum Chem. **36**, 217 (1989).

[63] S. Sorella and L. Capriotti, Algorithmic differentiation and the calculation of forces by quantum Monte Carlo, J. Chem. Phys. **133**, 234111 (2010).

[64] C. Filippi, R. Assaraf, and S. Moroni, Simple formalism for efficient derivatives and multi-determinant expansions in quantum Monte Carlo, J. Chem. Phys. **144**, 194105 (2016).

[65] J. van Rhijn, C. Filippi, S. De Palo, and S. Moroni, Energy derivatives in real-space diffusion Monte Carlo, J. Chem. Theory Comput. **18**, 118 (2022).

[66] S. Pathak and L. K. Wagner, A light weight regularization for wave function parameter gradients in quantum Monte Carlo, AIP Adv. **10**, 085213 (2020).

[67] P. J. Reynolds, R. Barnett, B. Hammond, R. Grimes, and W. Lester Jr, Quantum chemistry by quantum Monte Carlo: Beyond ground-state energy calculations, Int. J. Quantum Chem. **29**, 589 (1986).

[68] C. Lee, W. Yang, and R. G. Parr, Development of the Colle-Salvetti correlation-energy formula into a functional of the electron density, Phys. Rev. B **37**, 785 (1988).

[69] N. D. Mermin, Thermal properties of the inhomogeneous electron gas, Phys. Rev. **137**, A1441 (1965).

[70] https://github.com/giacomotenti/QMC_hugoniot.